OPEN

Citation: BoneKEy Reports **3**, Article number: 571 (2014) | doi:10.1038/bonekey.2014.66

www.nature.com/bonekey

ORIGINAL ARTICLE

Osteocyte expression of caspase-3, COX-2, IL-6 and sclerostin are spatially and temporally associated following stress fracture initiation

Andy C Wu[1,2], Lisa J Kidd[3], Nicholas R Cowling[3], Wendy L Kelly[1] and Mark R Forwood[1]

[1]School of Medical Science and Griffith Health Institute, Griffith University, Gold Coast Campus, Gold Coast, Queensland, Australia. [2]Mater Medical Research Institute, and UQ Translational Research Institute, Mater Hospital, Brisbane, Queensland, Australia. [3]School of Veterinary Science, The University of Queensland, Gatton, Queensland, Australia.

Stress fractures (SFxs) are debilitating injuries and exact mechanisms that initiate their repair incompletely understood. We hypothesised that osteocyte apoptosis and expression of cytokines and proteins such as sclerostin, VEGF, TGF-β, COX-2 and IL-6 were early signalling events to facilitate the formation of periosteal woven bone and recruitment of osteoclast precursors to the site of remodelling. A SFx was created in the right ulna of mature female wistar rats using cyclic end loading. Rats were killed 1, 4 and 7 days after loading ($n = 5$ per group). Standard histological staining was used to examine SFx morphology and immunohistochemistry to detect the localisation of these proteins and *in situ* hybridisation to detect mRNA along the SFx line or gene expression to quantify the target genes. Unloaded ulnae served as controls. The labelling index of caspase-3, COX-2 and IL-6 was significantly elevated in the region of SFxs at all time points compared with controls ($P < 0.001$). In addition, the labelling index of sclerostin protein was significantly reduced in osteocytes adjacent to the SFx region when compared with controls at all three time points ($P < 0.001$). Both VEGF and TGF-β expressions were only localised in the woven bone. These data reinforce the involvement of osteocyte apoptosis in the healing of fatigue damage in bone, and demonstrate that local regulation of sclerostin, COX-2 and IL-6 are important signalling events associated with new bone formation and SFx remodelling.

BoneKEy Reports **3**, Article number: 571 (2014) | doi:10.1038/bonekey.2014.66

Introduction

Repetitive cyclic loading has been widely adopted to investigate the influence of mechanical loading on bone formation[1–5] or the effect of fatigue loading on microdamage accumulation.[6–8] In the latter case, a load is applied to the bone until a predetermined index of failure is reached. Current evidence indicates that microdamage generated by loading of the rat ulna propagates rapidly to form a fatigue fracture.[1,7–11] Modifications of this model have been used to characterise the healing response of fatigue fracture.[9–12]

Fatigue fractures, otherwise known as stress fracture (SFx), are usually located in the weight bearing bones such as the metatarsals and tibiae of humans.[13,14] They are commonly found in humans and animals that engage intensively in repetitive physical activities. Immobilisation and rest are the common treatment for the management of SFx,[15] but the recovery time for complete healing is slow, resulting in the loss of productivity for the individuals involved. Elucidation of the molecular/signalling pathways involved during the repair response of SFx can extend our knowledge of their aetiology and assist in developing strategies to facilitate healing.

Periosteal woven bone formation is associated with early phase of SFx repair and its densification has an important role in restoring the strength of the damaged bone.[10] The magnitude of the woven bone response is also damage dependant.[16] Its repair has been described as a process of intramembranous fracture repair, with the induction of genes associated with angiogenesis, cell proliferation and osteoblastogenesis.[12] Conversely, repair of the SFx line itself proceeds via a process of direct bone remodelling, directed by gene expression for remodelling-related signalling.[9,17–19]

Osteocyte apoptosis has also been considered a possible mechanism to control the activation and targeting of osteoclastic resorption in response to bone fatigue.[17,20–22] Use of the ulna-loading model to study SFx identified that the distribution of apoptotic osteocytes was temporally linked with

Correspondence: Professor M Forwood, School of Medical Science, Griffith University, Gold Coast Campus, Parklands Drive, Gold Coast, Queensland 4222, Australia. E-mail: m.forwood@griffith.edu.au

Received 11 April 2014; revised 19 June 2014; accepted 1 July 2014; published online 3 September 2014

stress-induced damage.[20,22,23] We previously demonstrated the gene expression of key growth factors and cytokines associated with SFx repair,[9] but we had not associated that expression with the cellular localisation of the protein in tissue surrounding the SFx region.

Sclerostin, a protein expressed predominately by osteocytes, is a potent inhibitor of bone formation that is linked to the Wnt signalling pathway. The spatial tissue distribution of sclerostin associated with adaptive ulna loading has been described,[24] but not in relation to SFx repair. The localisation and expression of sclerostin in SFx region can provide some insight into its role for initiating healing. Transforming growth factor-beta 1 (TGF-β) a cytokine expressed abundantly in bone that stimulates matrix protein synthesis and can also influence cells that are responsible for bone modelling and remodelling.[25] In this study, our first aim was to determine whether osteocyte apoptosis, linked to the initiation of SFx, was spatially associated with sclerostin and TGF-β protein expression during the early phase of SFx healing.

We also identified upregulation of gene expression of several key cytokines, including interleukin 6 (IL-6; inflammatory and bone formation), cyclooxygenase 2 (COX-2; inflammation, bone formation) and vascular endothelial growth factor (VEGF; angiogenesis) during a time course of SFx healing. These cytokines are essential during fracture healing. For example in IL-6 knockout mice, the early phase of tibial fracture healing is associated with reduced osteoclastogenesis and impaired callus strength, when compared with wild-type controls.[26] In addition, prostaglandin inhibition delays SFx healing;[27] and angiogenesis is an essential process to provide blood flow to cells and growth factors to accelerate the healing response, and support remodelling.[18] The second aim of this study is to localise the messenger RNA (mRNA) and quantify the local protein distribution of these markers along the SFx region up to 1 week after loading of rat ulnae. We hypothesised that osteocytes or periosteal cells in the vicinity of the SFx express these markers to regulate the early repair of SFx.

Results

Fracture histology

All the animals subjected to the loading regime developed SFx. Longitudinal serial sections were obtained from the loaded ulnae 1, 4 and 7 days after loading. Longitudinal sections were selected to visualise the SFx along the complete fracture length, starting from the exit point at the periosteum into the intracortical region towards the medullary cavity. At 1 day post loading, the periosteum at the exit point of the fracture appeared undisturbed with typical stromal cells visible at the periosteal surface, with no visible woven bone or any callus structure present. However, by day 4, a heterogeneous population of cells was visible at the exit point of the fracture, which consists of matrix producing cells and mature osteoblast cells embedded in woven bone. The woven bone appeared porous and stretched along the periosteum at the fracture exit point. A developing periosteum was visible on the outer surface of the woven bone. By day 7, densification of woven bone began, with dramatically less osteoblasts, and osteoid visible within the mineralised bone matrix. Similar to day 4, a developing periosteum was formed on the outer surface of the woven bone. This observation is consistent with current histological characterisation of SFx using this model.[9,12]

Gene expression and caspase-3 localisation at the SFx region

Quantitative mRNA expression of caspase-3 in loaded ulnae over a 2-week period following loading were normalised to house-keeping genes. Their expression was compared with the normalised data from the ULC group (**Figure 1a**). Caspase-3 gene expression showed a significant increase in the SFx limbs when compared with the ULC. At 4 h after fracture, there was a 2.5-fold increase in the expression of caspase-3 and this level of expression was maintained until day 7 after loading. Peak mRNA expression was detected by 2 weeks after loading, with a

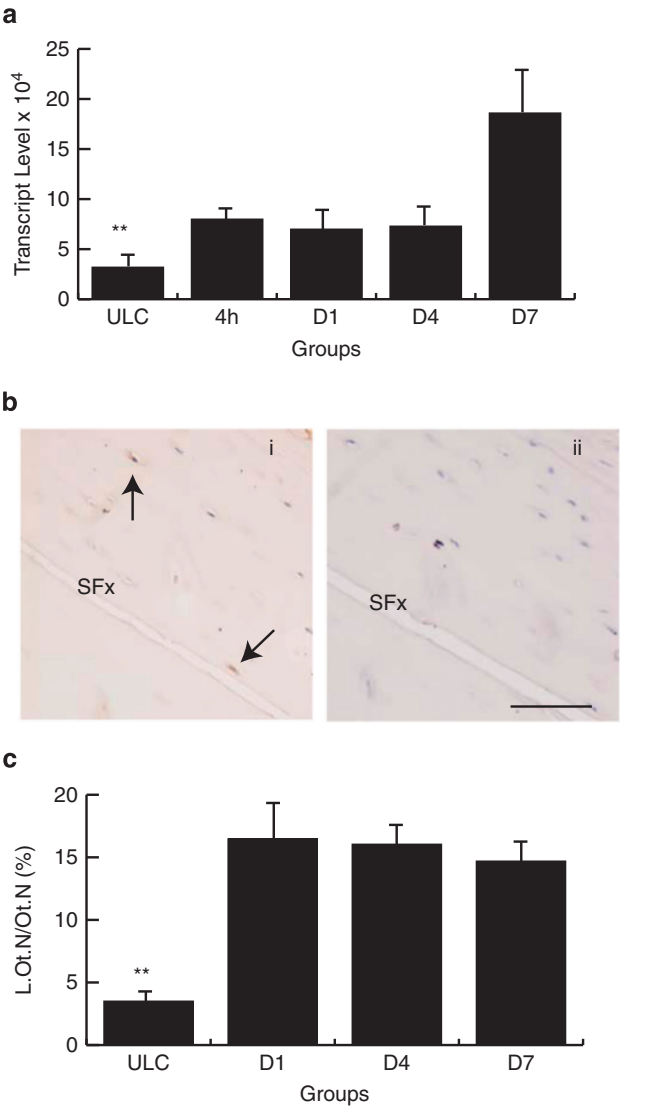

Figure 1 Caspase-3 gene and protein expression during early phase of SFx healing. Caspase-3 gene expression was significantly increased in right (loaded) ulnae from day 1 when compared with ULC ($P<0.05$) and peaked expression occurred by day 14 after the initiation of SFx (**a**). (**b**) Localisation of caspase-3 protein in osteocytes adjacent to the SFx at day 7 (**bi**). Isotype controls showed negative staining in this region (**bii**). The labelling indices (L.Ot.N/Ot.N, %) of osteocytes adjacent to the SFx across all time-points showed a dramatic increase in caspase-3 expression compared with ULC ($P<0.001$) (**c**). SFx, stress fracture, Scale bar, 50 μm.

fourfold increase in expression when compared with the ULC ($P<0.05$). Overall, gene expression of caspase-3 was significantly increased after initiation of SFx. Immunohistochemical analysis demonstrated caspase-3 protein was distributed in osteocytes across the intracortical area of all loaded ulnae (**Figure 1bi**), and in cells present in the marrow cavity (data not shown). In addition, caspase-3 staining was visible in the woven bone, suggesting that cells undergo rapid turnover through apoptosis and proliferation in that region (data not shown). Staining was also sparsely detected in osteocytes throughout the ulnar diaphysis. The isotype control was negative for non-specific staining (**Figure 1bii**). Histomorphometry analysis suggested that there were no significant differences between the labelling indices of caspase-3 in osteocytes across all three time-points. However, the labelling index of osteocytes was significantly elevated along the complete SFx length compared with ULC ($P<0.001$; **Figure 1c**). The labelling index of osteocytes adjacent to the SFx was also elevated when compared with the region distant from the SFx region (data not shown), suggesting that SFx induces the apoptosis of these cells.

Sclerostin staining was reduced in the SFx region

SOST mRNA was localised predominately in osteocytes in the SFx ulnae (**Figure 2a**). Positive immunolabelling was observed throughout the ulnae intracortical area and was expressed only by osteocytes, and not present in the marrow cavity (**Figure 2b**). Sclerostin staining was visible in osteocyte canaliculi, with dramatic weak staining of the canalicular network observed along the SFx line compared with ULC. At the SFx region, the labelling indices of sclerostin positive osteocytes was significantly reduced by ~40% compared with sclerostin positive osteocytes in the ULC ($P<0.001$, **Figure 2c**). This was also evident compared with the region distant from the SFx line of the same loaded ulnae (data not shown; see **Figure 2bii**). In addition, there is no significant difference between the labelling indices of sclerostin-positive osteocytes across all three time-points examined ($P>0.1$). These data suggest a reduction in expression of sclerostin in the region of SFx, which is the site where periosteal woven bone formation occurs.

COX-2 and IL-6 are expressed by osteocytes at SFx region

COX-2 mRNA was localised in the woven bone at SFx exit point and osteocytes adjacent to the SFx line. Sense control sections did not demonstrate a non-specific hybridisation signal at these locations (data not shown). Similar to its mRNA expression, COX-2 protein was localised throughout the intracortical bone area of the loaded limb, expressed in osteocytes and in cells of the marrow cavity and growth plate region. Moderate COX-2 staining was visible in the woven bone. When quantified, COX-2 adjacent to the SFx line, there were significant differences between the labelling indices of COX-2 in osteocytes adjacent to the SFx line, with its expression significantly decreased by day 7 (**Figure 3**, $P<0.01$). Both the labelling indices of osteocytes were significantly higher along the SFx line compared with ULC ($P<0.001$) (**Figure 3**) and cortical region distal to the SFx line in the same loaded ulnae (data not shown). The isotype control was negative for non-specific staining in these regions (not shown).

IL-6 followed a similar pattern of expression as COX-2, with IL-6 mRNA being localised in the periosteal woven bone and

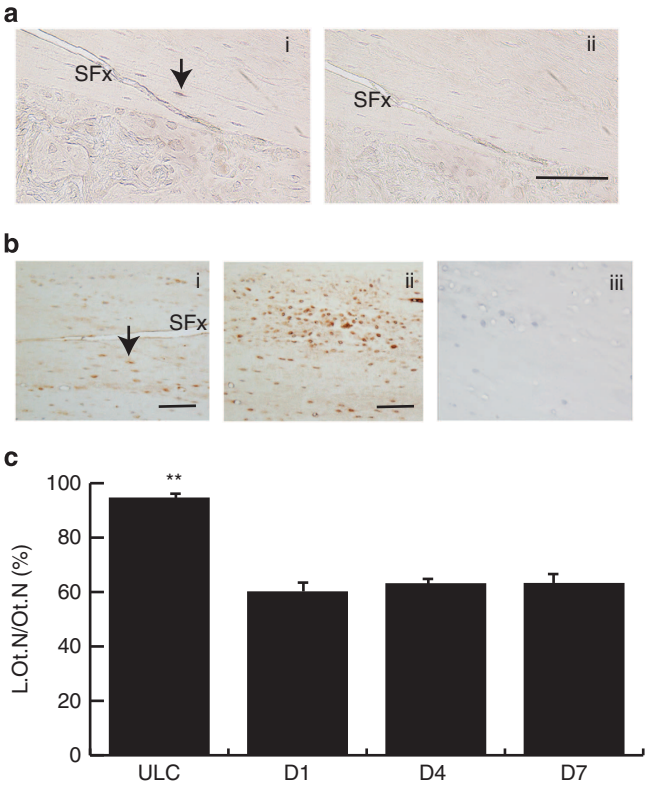

Figure 2 Localisation of SOST mRNA and protein in the SFx region. (**a**) SOST mRNA (**ai**) and sclerostin protein (**bi**) localised in osteocytes (arrows) adjacent to the SFx line. (**bii**) Shows sclerostin labelling at a site distant to the SFx line in the same section. Both anti-sense probe and isotype control were negative (**aii**, **biii**). (**c**) Labelling indices (L.Ot.N/Ot.N, %) of sclerostin protein were significantly reduced in the fracture region when compared with the ULC across all time-points (**c**, $P<0.001$). SFx, stress fracture. ULC, unloaded control. $^{**}P<0.001$, Scale bar, 50 μm.

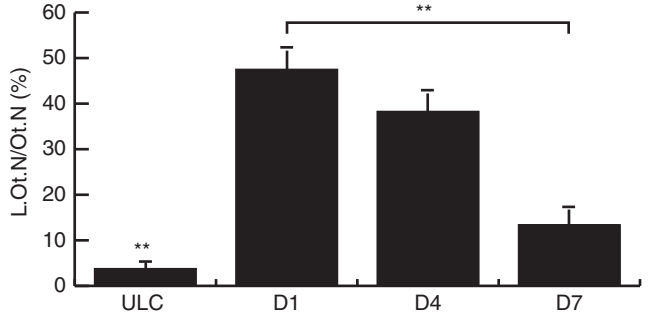

Figure 3 Labelling indices (L.Ot.N/Ot.N, %) of COX-2-positive osteocytes adjacent to the SFx showed a decrease in expression from day 1 (D1) to day 7 (D7) following SFx ($P<0.001$). COX-2-positive osteocytes were elevated at each time-point when compared with ULC. $^{**}P<0.001$.

weak expression detected in the osteocytes in the intra-cortical area. Sense control sections were negative for non-specific hybridisation (**Figure 4a**). IL-6 protein was localised throughout the woven bone and osteocytes (**Figure 4b**). Histomorphometry quantification of IL-6 along the SFx line identified upregulation of IL-6 protein in this region when compared with ULC (**Figure 4c**) and the region away from the SFx region in the loaded ulnae (data not shown). There were no significant

differences of osteocytes expressing IL-6 across the study time points.

Cells within the woven bone express various cytokines and growth factors

The expression of cytokine and growth factors were quantified in cells within the woven bone at the SFx exit point (**Table 1**). Insufficient woven bone for measurement was present at day 1 following loading. Caspase-3, COX-2, IL-6, VEGF and TGF-β can all be detected at the exit point of the SFx. Numerical density of both IL-6 and TGF-β showed a significant reduction in expression of positive cells in the woven bone from day 4 to 7 after loading, with the reduction of IL-6 from 209 ± 15 to 79 ± 27 cells mm^{-2} and TGF-β from 1230 ± 146 to 819 ± 36 cells mm^{-2}. There were no significant differences in the numerical density of caspase-3, COX-2 and VEGF at this location.

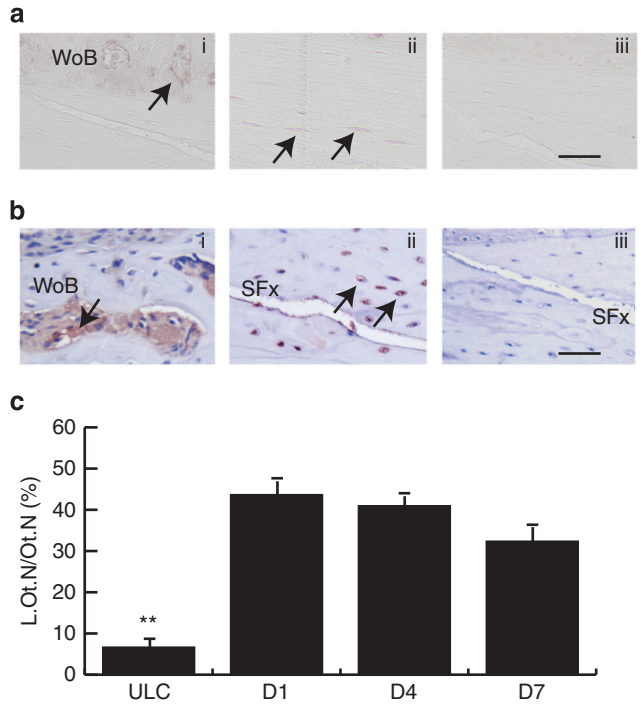

Figure 4 Localisation of IL-6 mRNA and protein in the SFx region. Localisation of both IL-6 mRNA and protein in the periosteal woven bone (**ai**, **bi**); and osteocytes adjacent to the SFx line (arrows, **aii**, **bii**). Both the anti-sense probe and isotype control were negative for nonspecific staining (**aiii**, **biii**). Labelling indices (L.Ot.N/Ot.N, %) of IL-6 protein were significantly elevated in the SFx region when compared with the ULC across all time points ((**c**), $P < 0.001$). SFx, stress fracture. ULC, unloaded control. $^{**}P < 0.001$. Scale bar, 50 μm.

Table 1 Quantification of IHC-positive cells in the woven bone at the periosteal surface at the SFx exit point

	Numerical Density (cells/mm²)		
IHC antigen	*Day 4*	*Day 7*	*Significance*
Caspase-3	1069 ± 123	985 ± 117	NS
COX-2	1471 ± 120	1167 ± 78	NS
IL-6	209 ± 15	79 ± 27	$P < 0.003$[a]
VEGF	836 ± 122	861 ± 81	NS
TGF-β	1230 ± 146	819 ± 36	$P < 0.026$

Abbreviations: IHC, immunohistochemistry; NS, not significant; SFx, stress fracture.
[a]Day 4 vs day 7, Student's *t*-test.

Discussion

Bone is a dynamic organ with the ability to repair itself when damaged via the process of fracture repair or direct bone remodelling.[9,12,28,29] Osteocytes are terminally differentiated osteoblasts that become embedded into the mineralised matrix secreted during bone formation. Due to their abundance and extensive communication networks, osteocytes are recognised as mechanosensors that detect mechanical strain and initiate chemical signalling for functional adaptation.[30] Our first objective was to confirm the distribution of apoptotic osteocytes surrounding the SFx line, consistent with other reports following ulnar loading.[20,22] We observed an expected increase in apoptotic osteocytes along the SFx line after SFx induction, but also identified a specific reduction in sclerostin protein expression within the SFx region. Other candidate molecules such as COX-2 and IL-6 were also significantly elevated in osteocytes within the SFx region, supporting osteocytic regulation of the early phase of SFx healing. TGF-β and VEGF protein were only localised in the woven bone in the SFx region, indicating a principal role in bone formation and vascularisation for expansion of the woven bone. The changes in tissue distribution of these molecules following SFx are consistent with observed changes in gene expression.[9,18]

Osteocyte apoptosis, adjacent to microdamage, has been extensively documented in rat ulnae following initiation of fatigue damage. Verborgt *et al.*[20] found a large number of TUNEL-positive cells surrounding the microdamage compared with sites distant from the damage,[20] and similar observations are reported by others (Follet *et al.*,[23] Kennedy *et al.*[31]). Cardoso *et al.*[17] also proposed that osteocyte apoptosis is necessary to initiate intracortical bone remodelling after fatigue microdamage. They observed that rats subjected to continuous exposure to a pan-caspase inhibitor completely blocked fatigue-induced apoptosis and osteoclastic remodelling after loading.[17] Osteoprotegerin, the competitive RANKL inhibitor, also declines, and RANKL increases at regions of microdamage where the greatest density of caspase-3-positive osteocytes are observed, confirming osteocyte regulation of remodelling events.[31] It is clear that fatigue-induced apoptosis is temporally associated with bone remodelling, and this targeted remodelling is central to maintaining structural integrity of bone. Our data confirm that osteocyte apoptosis is also linked with macroscopic bone damage such as SFx and that a decrease in sclerostin protein accompanies this response.

Sclerostin is an osteocyte-specific cysteine-knot secreted glycoprotein produced by the SOST gene. Mutation of the SOST gene leads to bone disorders in patients who exhibit very high bone mass.[32] We observed a localised reduction of sclerostin protein expression in the SFx region, when compared with the control. This reduction is evident as early as day 1 after loading, and may contribute to woven bone formation at the periosteum where SFx originated. It is unlikely that the reduction in sclerostin-positive osteocytes along the SFx is due to increased apoptosis of these cells, because the numerical

density of sclerostin-negative osteocytes was significantly higher than that of apoptotic cells. Significant reductions in sclerostin protein have been observed following adaptive ulnar loading by other groups.[24,33] The signalling mechanisms are slowly emerging and involve several pathways that mediate Wnt/LRP5,[24] including PGE_2[34] and TGF-β[25] that directly regulate sclerostin expression. In addition, IL-6 family cytokines act via gp130 in the osteoblast lineage to stimulate formation of osteoclasts,[35] activity of osteoblasts[36] and to inhibit expression of sclerostin.[37] The localised increase in IL-6 is therefore a likely candidate for osteocytic signalling that initiates many of the necessary events for periosteal stabilisation by woven bone and remodelling activation. In particular, IL-6 induces expression of monocyte chemotactic protein-1 (MCP-1) in many cell types,[38–40] and is consistent with the increased expression of MCP-1 following SFx[19] that promotes and supports remodelling activation via osteoclastogenesis.

In addition, COX-2 a key mediator of mechanically induced bone formation and SFx repair,[27,41] was elevated in osteocytes adjacent to the SFx within 24 h, and reduced by day 7. COX-2 promotes mesenchymal cell differentiation into osteoblast cells during skeletal repair.[42] But importantly, strain-induced *Sost* downregulation proceeds through COX-2-mediated PGE_2 signalling.[34] In the present study, we have provided the tissue localisation to support observations of increased gene expression of key signalling molecules following SFx initiation.[9] Together, the increased levels of osteocytic COX-2 and IL-6, and absence of osteocytic TGF-β, are consistent with their known regulation of *Sost*.[25,34,37] A limitation of our study is that we have not provided a mechanistic test of our hypothesis to support the role of these cytokines during early SFx repair, but we do now link the increased gene expression, previously reported, to specific cell localisation. We have provided confirmation of the role of osteocyte apoptosis, but also novel observations on SFx-specific regulation of sclerostin, COX-2 and IL-6 in osteocytes in the early repair response of SFx.

In conclusion, the initiation of SFx was associated with a significant localised reduction of sclerostin protein expression, but increased expression of IL-6 and COX-2, in osteocytes adjacent to the SFx region. These observations, in combination with increased localisation of TGF-β and VEGF at the periosteum, support our earlier observations of their gene expression associated with establishment of woven bone, and intracortical remodelling during the early phase of SFx healing.

Materials and Methods

Experimental animals

A total of 40 female Wistar rats of age 16–20 weeks with an average weight of 293 ± 3 g were used. Rats were housed in pairs and allowed *ad libitum* feeding and free cage activity in between loading sessions. The University of Queensland animal ethics committee approved the experimental ethics. A single subcutaneous injection of an opioid analgesic (Buprenorphine, 0.05 mg kg^{-1}) was used following each loading session. There were a total of three experimental groups subjected to loading of the right ulna and one unloaded control group (ULC, $n = 5$ per group) for immunohistochemistry. In separate group, 20 female wistar rats were used for *in situ* hybridisation, with three groups subjected to loading protocol ($n = 5$) and one as ULC group. Tissues were collected 1, 4 and 7 days post loading.

In vivo loading model

The fatigue loading model used in this study followed a similar loading regimen described elsewhere.[6,8,9] Isofluorane and oxygen general anaesthesia was used during loading. The right forelimbs of the rat were positioned in a custom-designed loading device[43] with axial cyclic loading applied to the ulnae. The loading device was attached to a linear vertical displacement transducer connected to a MacLab (AD Instruments, Colorado Springs, USA) and the displacement of the limb during loading was monitored using Chart v5.4 (AD Instruments). The load magnitude and haversine wave-form was confirmed by an oscilloscope connected to the load controller. The forelimbs were cyclically loaded using a 2 Hz haversine waveform to a compressive force of 17–24 N until a 10% increase in displacement was reached. The total number of loading cycles to achieve bone fatigue was 5496 ± 254 cycles. At 1, 4 and 7 days after loading, the rats were killed using CO_2 asphyxiation. Data were compared with ulnae from the ULC.

Gene expression

In a separate experiment, we performed quantitative real-time PCR to determine the temporal pattern of gene expression of caspase-3 during SFx repair. The RNA of loaded (right) and ULC ulnae were obtained from our previous study, and quantitative real-time PCR protocol followed our previous described method.[9] Quantitative real-time PCR was undertaken using pre-made TaqMan assay (Assay ID Rn00563902_m1; Applied Biosystems, Foster City, CA, USA) using the BioRad CFX96 real time PCR detection system (BioRad, Gladesville, NSW, Australia). The PCR cycling condition was as follows: 95 °C for 10 min to activate the taq polymerase, followed by 40 cycles of annealing and extension step at 95 °C for 15 s and 58 °C for 70 s. The expression of caspase-3 was expressed relative to the normalised expression of HPRT and GAPDH housekeeping genes (**Table 2**).

General histology of SFx region

At the end of each time point, a 10–15-mm section of the ulnae were excised with most of the surrounding soft tissues removed. The ulnae were processed for histological analysis by fixation in 4% paraformaldehyde made up in phosphate buffered saline for 24 h at 4 °C under vacuum. Specimens were then decalcified in 14% EDTA (pH 7.4) for 7 weeks and infiltrated with paraffin wax using a Shandon Citadel 1000 tissue processor (ThermoFisher Scientific, Scoresby, VIC, Australia) using standard protocols. After being embedded into paraffin blocks, 5-μm thick serial longitudinal sections were cut along the full length of the SFx line. Sections were stained with toluidine blue to observe the basic morphology of the SFx region.

Table 2 Taqman primers used for the detection of target genes in the experiment

Gene	*Applied Biosystems Assay ID*	*Amplicon size (bp)*
HPRT	Rn01527840_m1	64
GAPDH	Rn01775763_g1	174
Caspase-3	Rn00563902_m1	95

Table 3 primers used to amplify target genes for riboprobe synthesis

Gene	*Forward (5′-3′)*	*Reverse (5′-3′)*	*Size (bp)*
COX-2	GTCTAAATCGGGAGTTGGAATCA	CACAGTATGACACAACAGCCCA	501
IL-6	GACTGATGTTGTTGACAGCCAC	TAGCCACTCCTTCTGTGACTCT	509
SOST	TCAGAGAGTACCCAGAGCCT	TAGTAGGCGTTCTCCAGCTC	523

Riboprobe synthesis and *in situ* hybridisation

Complementary DNA plasmid templates for *in situ* hybridisation were generated by using PCR to amplify SOST, COX-2 and IL-6 sequences from rat bone or kidney complementary DNA using specific primers (**Table 3**). The DIG labelling system (Roche Australia, Castle Hill, NSW, Australia) was employed to label the riboprobe. The process for riboprobe synthesis and *in situ* hybridisation followed our previous established methods.[9,19] The sections were mounted in 0.2% propyl gallate in phosphate buffered saline/50% glycerol with no counterstain. Control sections included the sense probe and omission of probes or anti-digoxigenin-AP antibody.

Immunohistochemistry

Immunohistochemistry was performed on deparaffinised and rehydrated sections as described previously.[9,19] Specific primary antibodies were used in this study which includes: caspase-3 (rabbit polyclonal, Santa Cruz Biotechnology, Dallas, TX, USA), sclerostin (goat anti-mouse, R&D Systems, Minneapolis, MN, USA), COX-2 (goat anti-rat, Santa Cruz), IL-6 (rabbit polyclonal, Abcam, Melbourne, VIC, Australia), VEGF (Santa Cruz), TGF-β (Abcam). The relevant isotype control antibodies include normal rabbit immunoglobulin-G (IgG) and normal goat IgG. All sections were counterstained with Mayer's hematoxylin (Sigma-Aldrich, Castle Hill, NSW, Australia) and mounted using permanent mounting medium (Cytoseal 60, ProSciTech, Townsville, QLD, Australia).

Histomorphometry

Sections were examined using bright field optics on an Olympus BX60 microscope (Olympus, Macquarie Park, NSW, Australia). Classification of cells was based on morphology and all the immunostained sections were counterstained with haematoxylin to allow visual identification of the cells. At the intracortical surface, the total number of osteocytes (Ot.N) comprised the number of labelled osteocytes (L.Ot.N) plus the non-labelled osteocytes along the SFx line. The percentage of labelled osteocytes (labelling index) was then calculated (L.Ot.N/Ot.N, %). Osteocytes positive for sclerostin and caspase-3 protein were quantified within the width of one optical field (250 μm) that included the SFx line, along the full length of the SFx at a magnification of × 400, giving a total of six optical fields per specimen. Osteocytes in the ULC ulna at the equivalent anatomical location to the SFx; and, an area distal from the fracture region in the loaded ulnae were also quantified and served as control.

Statistical analysis

Data were analysed using SPSS 17.0 (SPSS Inc., IBM Australia, St Leonards, NSW, Australia). Differences among groups in gene expression and labelling index of intracortical osteocytes were analysed using one-way analysis of variance with *post-hoc* analysis of between group differences using Fisher's protected least significant difference. For woven bone analysis, differences between groups for labelling index were tested using Student's *t*-test. Significance was determined at $P < 0.05$. Probability levels between 0.05 and 0.1 were classified as marginally significant if the difference between means was greater than 2 × the standard error of measurement.

Conflict of Interest

The authors declare no conflict of interest.

Acknowledgements

This work was funded in part by NHMRC Project Grants 401553, 1049190 and 511187; and The Rebecca L Cooper Medical Research Foundation. We thank Mr Bradley Paterson for his expert technical assistance.

References

1. Silva MJ, Touhey DC. Bone formation after damaging in vivo fatigue loading results in recovery of whole-bone monotonic strength and increased fatigue life. *J Orthop Res* 2007;**25**:252–261.
2. Chow JW, Jagger CJ, Chambers TJ. Characterization of osteogenic response to mechanical stimulation in cancellous bone of rat caudal vertebrae. *Am J Physiol* 1993;**265**(2 Pt 1): E340–E347.
3. Rubin CT, Pratt GW, Porter AL, Lanyon LE, Poss R. The use of ultrasound *in vivo* to determine acute change in the mechanical properties of bone following intense physical activity. *J Biomech* 1987;**20**:723–727.
4. Torrance AG, Mosley JR, Suswillo RF, Lanyon LE. Noninvasive loading of the rat ulna *in vivo* induces a strain-related modeling response uncomplicated by trauma or periostal pressure. *Calcif Tissue Int* 1994;**54**:241–247.
5. Turner CH, Forwood MR, Rho JY, Yoshikawa T. Mechanical loading thresholds for lamellar and woven bone formation. *J Bone Miner Res* 1994;**9**:87–97.
6. Bentolila V, Boyce TM, Fyhrie DP, Drumb R, Skerry TM, Schaffler MB. Intracortical remodeling in adult rat long bones after fatigue loading. *Bone* 1998;**23**:275–281.
7. Danova NA, Colopy SA, Radtke CL, Kalscheur VL, Markel MD, Vanderby R *et al.* Degradation of bone structural properties by accumulation and coalescence of microcracks. *Bone* 2003;**33**:197–205.
8. Tami AE, Nasser P, Schaffler MB, Knothe Tate ML. Noninvasive fatigue fracture model of the rat ulna. *J Orthop Res* 2003;**21**:1018–1024.
9. Kidd LJ, Stephens A, Kuliwaba JS, Fazzalari NL, Wu AC, Forwood MR. Temporal pattern of gene expression and histology of stress fracture healing. *Bone* 2010;**46**:369–378.
10. Uthgenannt BA, Kramer MH, Hwu JA, Wopenka B, Silva MJ. Skeletal self-repair: stress fracture healing by rapid formation and densification of woven bone. *J Bone Miner Res* 2007;**22**: 1548–1556.
11. Uthgenannt BA, Silva MJ. Use of the rat forelimb compression model to create discrete levels of bone damage *in vivo*. *J Biomech* 2007;**40**:317–324.
12. Wohl GR, Towler DA, Silva MJ. Stress fracture healing: fatigue loading of the rat ulna induces upregulation in expression of osteogenic and angiogenic genes that mimic the intramembranous portion of fracture repair. *Bone* 2009;**44**:320–330.
13. Hallel T, Amit S, Segal D. Fatigue fractures of tibial and femoral shaft in soldiers. *Clin Orthop Relat Res* 1976;**118**:35–43.
14. Milgrom C, Finestone A, Sharkey N, Hamel A, Mandes V, Burr D *et al.* Metatarsal strains are sufficient to cause fatigue fracture during cyclic overloading. *Foot Ankle Int* 2002;**23**:230–235.
15. Boden BP, Osbahr DC. High-risk stress fractures: evaluation and treatment. *J Am Acad Orthop Surg* 2000;**8**:344–353.
16. Lynch JA, Silva MJ. *In vivo* static creep loading of the rat forelimb reduces ulnar structural properties at time-zero and induces damage-dependent woven bone formation. *Bone* 2008;**42**:942–949.

17. Cardoso L, Herman BC, Verborgt O, Laudier D, Majeska RJ, Schaffler MB. Osteocyte apoptosis controls activation of intracortical resorption in response to bone fatigue. *J Bone Miner Res* 2009;**24**:597–605.
18. McKenzie JA, Bixby EC, Silva MJ. Differential gene expression from microarray analysis distinguishes woven and lamellar bone formation in the rat ulna following mechanical loading. *PLoS ONE* 2011;**6**:e29328.
19. Wu AC, Morrison NA, Kelly WL, Forwood MR. MCP-1 expression is specifically regulated during activation of skeletal repair and remodeling. *Calcif Tissue Int* 2013;**92**:566–575.
20. Verborgt O, Gibson GJ, Schaffler MB. Loss of osteocyte integrity in association with microdamage and bone remodeling after fatigue in vivo. *J Bone Miner Res* 2000;**15**:60–67.
21. Noble BS, Peet N, Stevens HY, Brabbs A, Mosley JR, Reilly GC *et al.* Mechanical loading: biphasic osteocyte survival and targeting of osteoclasts for bone destruction in rat cortical bone. *Am J Physiol Cell Physiol* 2003;**284**:C934–C943.
22. Verborgt O, Tatton NA, Majeska RJ, Schaffler MB. Spatial distribution of Bax and Bcl-2 in osteocytes after bone fatigue: complementary roles in bone remodeling regulation? *J Bone Miner Res* 2002;**17**:907–914.
23. Follet H, Li J, Phipps RJ, Hui S, Condon K, Burr DB. Risedronate and alendronate suppress osteocyte apoptosis following cyclic fatigue loading. *Bone* 2007;**40**:1172–1177.
24. Robling AG, Niziolek PJ, Baldridge LA, Condon KW, Allen MR, Alam I *et al.* Mechanical stimulation of bone *in vivo* reduces osteocyte expression of Sost/sclerostin. *J Biol Chem* 2008;**283**:5866–5875.
25. Nguyen J, Tang SY, Nguyen D, Alliston T. Load regulates bone formation and Sclerostin expression through a TGFbeta-dependent mechanism. *PLoS ONE* 2013;**8**:e53813.
26. Wallace A, Cooney TE, Englund R, Lubahn JD. Effects of interleukin-6 ablation on fracture healing in mice. *J Orthop Res* 2011;**29**:1437–1442.
27. Kidd LJ, Cowling NR, Wu AC, Kelly WL, Forwood MR. Selective and non-selective cyclooxygenase inhibitors delay stress fracture healing in the rat ulna. *J Orthop Res* 2013;**31**:235–242.
28. Burr DB, Forwood MR, Fyhrie DP, Martin RB, Schaffler MB, Turner CH. Bone microdamage and skeletal fragility in osteoporotic and stress fractures. *J Bone Miner Res* 1997;**12**:6–15.
29. Mori S, Burr DB. Increased intracortical remodeling following fatigue damage. *Bone* 1993;**14**:103–109.
30. Marotti G. The osteocyte as a wiring transmission system. *J Musculoskelet Neuronal Interact* 2000;**1**:133–136.
31. Kennedy OD, Herman BC, Laudier DM, Majeska RJ, Sun HB, Schaffler MB. Activation of resorption in fatigue-loaded bone involves both apoptosis and active pro-osteoclastogenic signaling by distinct osteocyte populations. *Bone* 2012;**50**:1115–1122.
32. Li X, Ominsky MS, Niu QT, Sun N, Daugherty B, D'Agostin D *et al.* Targeted deletion of the sclerostin gene in mice results in increased bone formation and bone strength. *J Bone Miner Res* 2008;**23**:860–869.
33. Robling AG, Bellido T, Turner CH. Mechanical stimulation *in vivo* reduces osteocyte expression of sclerostin. *J Musculoskelet Neuronal Interact* 2006;**6**:354.
34. Galea GL, Sunters A, Meakin LB, Zaman G, Sugiyama T, Lanyon LE *et al.* Sost down-regulation by mechanical strain in human osteoblastic cells involves PGE2 signaling via EP4. *FEBS Lett* 2011;**585**:2450–2454.
35. Ishimi Y, Miyaura C, Jin CH, Akatsu T, Abe E, Nakamura Y *et al.* IL-6 is produced by osteoblasts and induces bone resorption. *J Immunol* 1990;**145**:3297–3303.
36. Bellido T, Borba VZ, Roberson P, Manolagas SC. Activation of the Janus kinase/STAT (signal transducer and activator of transcription) signal transduction pathway by interleukin-6-type cytokines promotes osteoblast differentiation. *Endocrinology* 1997;**138**:3666–3676.
37. Walker EC, McGregor NE, Poulton IJ, Solano M, Pompolo S, Fernandes TJ *et al.* Oncostatin M promotes bone formation independently of resorption when signaling through leukemia inhibitory factor receptor in mice. *J Clin Invest* 2010;**120**:582–592.
38. Arendt BK, Velazquez-Dones A, Tschumper RC, Howell KG, Ansell SM, Witzig TE *et al.* Interleukin 6 induces monocyte chemoattractant protein-1 expression in myeloma cells. *Leukemia* 2002;**16**:2142–2147.
39. Klouche M, Bhakdi S, Hemmes M, Rose-John S. Novel path to activation of vascular smooth muscle cells: up-regulation of gp130 creates an autocrine activation loop by IL-6 and its soluble receptor. *J Immunol* 1999;**163**:4583–4589.
40. Biswas P, Delfanti F, Bernasconi S, Mengozzi M, Cota M, Polentarutti N *et al.* Interleukin-6 induces monocyte chemotactic protein-1 in peripheral blood mononuclear cells and in the U937 cell line. *Blood* 1998;**91**:258–265.
41. Forwood MR. Inducible cyclo-oxygenase (COX-2) mediates the induction of bone formation by mechanical loading in vivo. *J Bone Miner Res* 1996;**11**:1688–1693.
42. Zhang X, Schwarz EM, Young DA, Puzas JE, Rosier RN, O'Keefe RJ. Cyclooxygenase-2 regulates mesenchymal cell differentiation into the osteoblast lineage and is critically involved in bone repair. *J Clin Invest* 2002;**109**:1405–1415.
43. Forwood MR, Bennett MB, Blowers AR, Nadorfi RL. Modification of the *in vivo* four-point loading model for studying mechanically induced bone adaptation. *Bone* 1998;**23**:307–310.